

Non-axisymmetric oscillations of roAp stars

L. Bigot¹, J. Provost¹, G. Berthomieu¹, W.A. Dziembowski², and P.R. Goode³

¹ Département Cassini, UMR CNRS 6529, Observatoire de la Côte d'Azur, B.P. 4229, 06304 Nice CEDEX 4, France

² Warsaw University Observatory, Al Ujazdowskie 4, 00-478 Warszawa, Poland; N. Copernicus Astronomical Center, Polish Academy of Science, Bartycka 18, 00-716 Warszawa, Poland

³ Big Bear Solar Observatory, New Jersey Institute of Technology, 40386 North Shore Lane, Big Bear City, CA 92314, USA

Received 18 October 1999 / Accepted 13 December 1999

Abstract. We calculate the effect of a strong dipole magnetic field on non-axisymmetric oscillations for roAp stars, with a typical range of photospheric magnetic fields B_p [0.5–1.5] kG. As Dziembowski & Goode (1996), we find that the oscillations are strongly affected by such magnetic fields in two different ways. The first one concerns the stability of modes, which are damped due to dissipation by Alfvénic waves. It leads to a small imaginary part of the frequency, about (1–15 μHz). The real part of the frequencies is also affected and is greater in the presence of magnetic field, with a shift of about 1–20 μHz . We find that these shifts are strongly influenced by the geometry of the mode, i.e. the value of the degree ℓ , as it has already been shown by Dziembowski & Goode (1996), and also by m , the azimuthal degree, with a significant amplitude. The magnetic field, because it breaks the spherical symmetry of the problem, raises partially the $(2\ell + 1)$ degeneracy of frequency in m . We find that the shift of both the real and imaginary parts is always greater than in the case of axisymmetric oscillations ($m = 0$), except for sectoral modes ($\ell = m$), for which the imaginary part is smaller. The second effect of large magnetic fields is to complicate the mode identification. The perturbations cannot be represented by pure single spherical harmonic, but by a series of harmonics due to the angular dependence of the Lorentz force. It is shown that this mixing of spherical harmonics also depends on the value of m . However, our calculations do not explain the observed selection of dipole modes in roAp stars, aligned with the magnetic axis, since they do not minimize energy losses due to Alfvénic waves.

Key words: stars: magnetic fields – stars: oscillations – stars: chemically peculiar – stars: interiors

1. Introduction

The roAp stars are a special subgroup of Ap stars which show rapid light variations. Since their discovery by Kurtz (1982), their number has grown to about 30. They are cold Ap stars ($T_{eff} \sim 8000 K$) having anomalous surface element abundances of Sr, Cr and Eu. With a mass of about $2 M_{\odot}$, they lie in the HR diagram at the intersection between the δ -Scuti instability strip and the main sequence. One important particularity of these

stars is the presence of a strong magnetic field of about kilogauss amplitude, discovered first by Babcock (1947). It has roughly a dipolar geometry, see Borra et al. (1982).

From the asteroseismological point of view, these roAp stars constitute a specific class of variable stars: they oscillate with high frequencies, say with large radial orders from 10 up to about 30. This represents a range of periods from 6 to 14 minutes, similar to the 5-minute oscillations of the Sun, but with much higher amplitude light variations (about 1 mmag). Recent discoveries by Martinez (1999) and Martinez et al. (1999) show possible long periods of 30 and 29 min, in two roAp stars, HD 75425 and HD 13038 respectively. However, as in most cases, roAp stars have rapid light variations, we assume, in this paper, high frequencies for oscillations. Another particularity is the geometry of these oscillations, which are aligned with the magnetic axis. They appear essentially as dipole modes, characterized by a spherical harmonic whose degree is $\ell = 1$ and an azimuthal degree $m = 0$, say with the same geometry as the magnetic field. Reviews on roAp stars are available in Kurtz (1990) and Matthews (1991). Recent theoretical works about roAp stars are discussed in Cunha (1998).

Any seismological study of roAp stars must take into account the presence of this strong magnetic field. A lot of studies have been done to explain the seismological observations of these objects. However, they have been limited to the linear and adiabatic approximations. Even in this case, the difficulties due to the magnetic field remain numerous. Roberts & Soward (1983) developed analytical solutions of the problem but for polytropic star models and for a weak magnetic field (≤ 0.1 kG), whose angular dependence has been neglected. They introduced the concept of the magnetic boundary layer and the possibility of Alfvénic wave production as a source of damping for p-modes. Campbell & Papaloizou (1986) considered numerically the general problem, taking into account the angular dependence of the Lorentz force, still in the case of polytropic models. However, they solved the problem for each colatitude. The global problem was first treated by Dziembowski & Goode (1996), who considered non-radial axisymmetric stellar oscillations, with strong magnetic fields still in the case of the magnetic boundary layer concept. They have shown that the frequencies are shifted by the magnetic field in a range of 10–20 μHz , for

the real part of the frequency, and $2 - 10\mu Hz$ for the imaginary part due to Alfvénic waves. They also showed that the modes of oscillations are not pure single harmonics but a mixing of them due to the angular dependence of the Lorentz force inside the magnetic layer. These results are consistent with the observations of HR 3831, whose frequency spectrum has been described by Kurtz (1992) as a sum of spherical harmonics of low degrees. Recently Cunha & Gough (1998) presented an alternative approach based on degenerate perturbation theory.

The aim of the present paper is to generalize the work of Dziembowski & Goode (1996) to non-axisymmetric oscillations, i.e. with the possibility of azimuthal dependence of modes and for magnetic fields up to 1.5 kG. We still use the same assumptions: we neglected non-adiabatic processes, like excitation, radiative damping, coupling with convection, and the effect of rotation.

2. The magnetic boundary layer approach

In the presence of a magnetic field the full set of equations describing stellar oscillations is very complicated to solve because of the Lorentz force. Hence, we adopted the concept of a magnetic boundary layer used in previous papers dealing with this problem, (Roberts & Soward 1983; Campbell & Papaloizou 1986; Dziembowski & Goode 1996). Although the magnetic field is strong everywhere inside the star, the Lorentz force has an influence on the dynamics of the oscillations only in the outer parts, where the density becomes so small that the magnetic pressure is of the same order as (or larger than) the gas pressure.

Let us define the ratio

$$\beta = \frac{B_p^2}{4\pi\Gamma_1 p} = \frac{v_A^2}{c_S^2}. \quad (1)$$

Γ_1 is the adiabatic exponent, p the unperturbed gas pressure. v_A and c_S are respectively the Alfvénic and sound speeds, and B_p the photospheric magnetic field (0.5-1.5 kG).

We can divide the star into two regions. The magnetic pressure is neglected compared with the gas pressure in the whole star (where $\beta \ll 1$), except in the very thin layer near the photosphere where $\beta \geq 1$. This thin layer, where β is non-negligible compared with the unit, is called the boundary magnetic layer. Inside this layer, there are no pure p-modes but rather the so-called magneto-sonic modes whose properties are a mixture of acoustic and Alfvénic modes. The bottom of this layer, r_{fit} , is chosen where the quantity β is sufficiently small to neglect the magnetic pressure and to provide a decoupling between p-modes and the magnetic field (see Table 1 in Appendix A). Then, to find the eigen-modes of the star, we must solve two systems of equations. Inside the star ($r \leq r_{\text{fit}}$), we solve the system for adiabatic p-modes oscillations without a magnetic field, described for example in Unno et al. (1989). In the magnetic layer, we integrate the complete system of ideal MHD equations still in the case of adiabatic oscillations (see appendix A). The advantage of this method is that, since this layer is very thin and situated at the top of the star, we can adopt a plane-parallel ap-

proximation, i.e. we neglect, locally, the curvature of the star. Assuming that the horizontal wave number remains small compared with the radial wave number, i.e. for small values of ℓ . We neglect the derivatives with respect to the colatitude θ for the perturbed quantities. Matching the solutions of the magnetic layer with the solutions of the deep interior, i.e. corresponding to non-magnetic oscillations, one obtains the eigen frequency spectrum of the star.

2.1. The magnetic layer

We divided the magnetic layer into a mesh in the colatitude θ , and we solved the MHD system of equations for each colatitude point with this plane-parallel approach.

The magnetic field is assumed to be dipolar which is a good approximation for Ap stars (Borra et al. 1982)

$$\vec{B}_0 = \frac{B_p}{x^3} (\cos\theta \vec{e}_r + \frac{\sin\theta}{2} \vec{e}_\theta) \quad (2)$$

x being the dimensionless radial position ($x = r/R$).

In our non-axisymmetric treatment, the displacement is given by

$$\vec{\xi} = r\{y(x, \theta) \vec{e}_r + z(x, \theta) \vec{e}_\theta + w(x, \theta) \vec{e}_\phi\} e^{im\phi} e^{i\omega t} \quad (3)$$

where ω is the pulsation of the acoustic mode, m the azimuthal order and ϕ the longitudinal angle. Another unknown quantity is the relative perturbation of the pressure

$$\frac{\delta p}{p} = q(x, \theta) e^{im\phi} e^{i\omega t}. \quad (4)$$

The Eulerian perturbation of the Lorentz force in the case of MHD approximation is

$$\vec{L} = 1/4\pi(\vec{\nabla} \wedge \vec{B}_1) \wedge \vec{B}_0 \quad \text{with} \quad \vec{B}_1 = \vec{\nabla} \wedge (\vec{\xi} \wedge \vec{B}_0) \quad (5)$$

In the magnetic layer we neglected all the derivatives by θ compared to the derivatives by x and we assumed large radial wave numbers, since we study high frequency oscillations. Then one gets the following form for the Lorentz force,

$$L_r = \frac{B_p^2}{8\pi R} \left(\frac{\partial^2 h}{\partial x^2} + im \frac{\sin\theta}{2} \frac{\partial w}{\partial x} \right) \quad (6)$$

$$L_\theta = -\frac{B_p^2}{4\pi R} \cot\theta \left(\frac{\partial^2 h}{\partial x^2} + im \frac{\sin\theta}{2} \frac{\partial w}{\partial x} \right) \quad (7)$$

$$L_\phi = \frac{B_p^2}{4\pi R \sin\theta} \left(\frac{im}{2} \frac{\partial h}{\partial x} - \cos^2\theta \sin\theta \frac{\partial^2 w}{\partial x^2} \right) \quad (8)$$

where

$$h = y \frac{\sin^2\theta}{2} - z \sin\theta \cos\theta. \quad (9)$$

In the case of non-axisymmetric oscillations, L_ϕ is not equal to zero, therefore the full system to solve contains the equation of motion projected on \vec{e}_ϕ . Then, this system for adiabatic motions

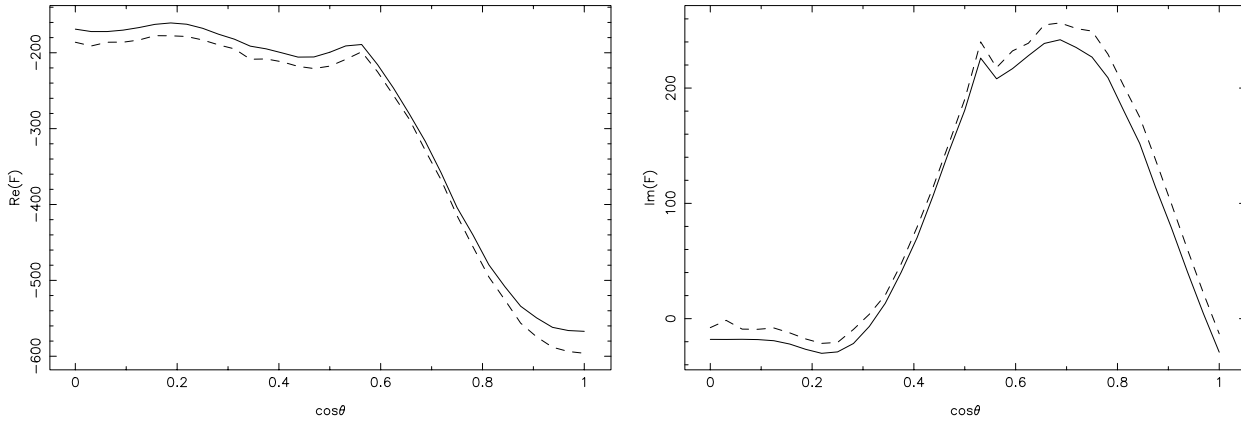


Fig. 1. (left) Real part of $\mathcal{F}(\theta, \omega, m)$, (right) the imaginary part of $\mathcal{F}(\theta, \omega, m)$ as functions of $\cos \theta$ for frequencies corresponding to a mode such as $n = 24$, $\ell = 1$ and for two values of m : $m = 0$ (full line) and $m = 1$ (dashed line). The magnetic field is $B_p = 0.7$ kG.

which was of the fourth order in the axisymmetric case (see Dziembowski & Goode 1996) becomes of the sixth order (see in Appendix A).

We assume small perturbations which leads us to linearize these equations. More details about this system are given in Appendix A. The result of this integration in the magnetic layer, with adequate boundary conditions at the top of the star, leads to the ratio $\mathcal{F}(\theta, \omega, m)$ between q_p and y_p the Lagrangian perturbation of pressure and the radial displacement for p-modes at x_{fit}

$$q_p(x_{\text{fit}}, \theta) = \mathcal{F}(\theta, \omega, m)y_p(x_{\text{fit}}, \theta) \quad (10)$$

This relation is then used as a boundary condition to solve numerically the classical system of equations, say without a magnetic field, for the inner part of the star, $x \leq x_{\text{fit}}$. The function $\mathcal{F}(\theta, \omega, m)$ only depends on the absolute value of m , because of the azimuthal symmetry of the unperturbed magnetic field. Therefore, the perturbations of the frequencies, due to the magnetic field, will depend also on the absolute value of m .

In Fig. 1, we can see two plots of the function \mathcal{F} which represent its real and imaginary parts, for a given radial order $n = 24$. We see that this function depends on m , for both the real and the imaginary parts. This implies that the corresponding eigen frequencies will also depend on m . The angular dependence of \mathcal{F} in θ is influenced by the angular dependence of the “acoustic cut-off frequency”, i.e. the maximal frequency for trapped p-modes. It follows from the expression Eq. A.22 in Appendix A that this frequency is

$$\omega_{ac} = \frac{c_S}{2H} \sqrt{\frac{1}{1 + \frac{\tan^2 \theta}{4}}} \quad (11)$$

with H the pressure scale height. Note from Eq. A.22 that when $\tan^2 \theta \geq \tan^2 \theta_0$

$$\tan^2 \theta_0 = 4 \left(\frac{\omega_{ac,0}^2}{\omega^2} - 1 \right) \quad \text{with} \quad \omega_{ac,0} = \frac{c_S}{2H} \quad (13)$$

the acoustic waves, at the top of the boundary layer, become partially propagating in the atmosphere. The equality in Eq. 12

corresponds to a null wave number and for $\theta = \theta_0$. Then, for a given frequency we have two regions in colatitude: from the pole to θ_0 the acoustic waves are reflected whereas for θ_0 to the equator they are partially propagating. This change of the mode’s nature has a signature in the behaviour of the function $\mathcal{F}(\theta, \omega, m)$. In the case of Fig. 1 $\cos \theta_0 \approx 0.6$.

Note that ω_{ac} is equal to the non-magnetic frequency $\omega_{ac,0}$ at the pole, and is smaller than $\omega_{ac,0}$ everywhere else. For the limiting case of the equator, it is equal to zero: therefore, there are no trapped waves at the equator.

2.2. The interior

Following Roberts & Soward (1983), there is a full decoupling between Alfvénic and acoustic modes for $x \leq x_{\text{fit}}$. This decoupling is recovered from Eq. A.10 and A.12 in Appendix A because of the small value of β . The Alfvénic modes are assumed to be dissipated well before the center of the star $r = 0$. A WKB treatment has been adopted to find them.

The p-modes are described by the system of equations without a magnetic field, as presented in Unno et al. (1989), whose solutions are y_ℓ, q_ℓ the radial displacement and the Lagrangian perturbation of the pressure. ℓ is the degree of the spherical harmonic $Y_\ell^m = P_\ell^m e^{im\phi}$. However, as the boundary condition $\mathcal{F}(\theta, \omega, m)$ depends on θ , the solutions are no longer represented by a single Y_ℓ^m , but by linear combinations of associated Legendre functions,

$$y_p(x, \theta) = \left(\sum_{k=m}^{nl} D_{km} y_k(x) P_k^m(\cos \theta) \right) \quad (14)$$

$$q_p(x, \theta) = \left(\sum_{k=m}^{nl} D_{km} q_k(x) P_k^m(\cos \theta) \right). \quad (15)$$

D_{km} represents the coefficient of angular mixing, it corresponds to the “weight” of each P_k^m in the sum. nl is the maximal degree of the Legendre functions in the series.

The effect of magnetic field on p-modes, in the interior, is described through the coefficients D_{km} .

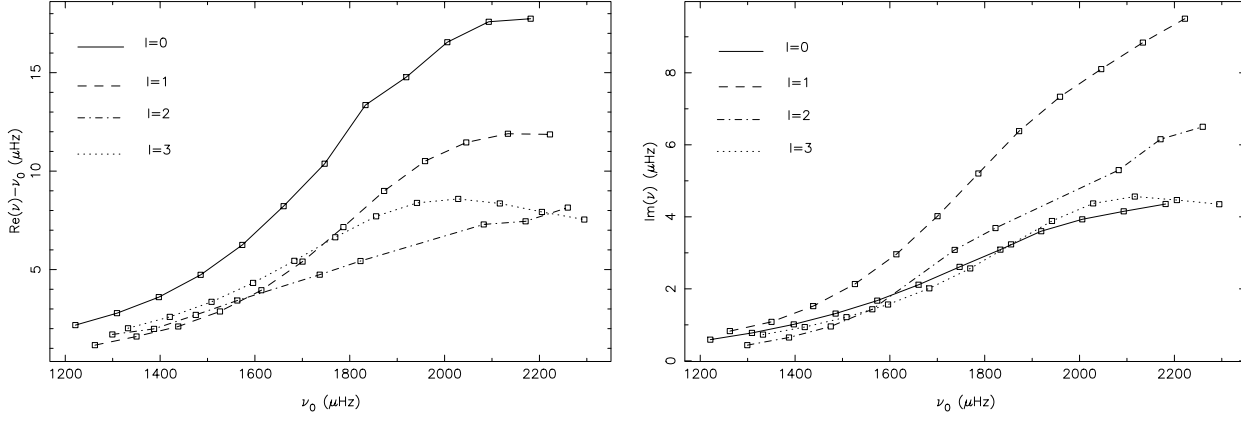


Fig. 2. Shift of the real part (left) and the imaginary part (right) of a set of non-magnetic frequencies ν_0 , for several degrees ℓ in the case of axisymmetric oscillations. These two sets of curves are plotted for a 1.0 kG magnetic field.

Then, the upper boundary condition Eq. 10 becomes,

$$\sum_{k=m}^{nl} D_{km} \{q_k(x_{\text{fit}}) \delta_{kk'} - y_k(x_{\text{fit}}) \mathcal{F}_{kk',m}(\omega)\} = 0 \quad (16)$$

with,

$$\mathcal{F}_{kk',m} = 4\pi \int_0^1 P_k^m(\cos\theta) \mathcal{F}(\theta, \omega, m) P_{k'}^m(\cos\theta) d(\cos\theta) \quad (17)$$

We use here the following normalization for Y_ℓ^m ,

$$\int Y_k^m \left(Y_{k'}^{m'}\right)^* d(\cos\theta) d\phi = \delta_{kk'} \delta_{mm'} \quad (18)$$

with $\delta_{kk'}$ the Kronecker symbol.

The relation in Eq. 16 (with k' taking the same values as k) is a homogeneous system whose solutions are the coefficients D_{km} . Its discriminant has to be equal to zero for eigen frequencies (for non-trivial solutions D_{km}). This last condition is used to find the frequency spectrum of the star.

Because $\mathcal{F}(\theta, \omega, m)$ is even in $\cos\theta$ (see the system in appendix A; it only depends on $\cos^2\theta$), the function $\mathcal{F}_{kk',m}$ does not vanish if k and k' have the same parity. In order to have a non-zero $\mathcal{F}_{kk',m}$, one must choose for the series Eq. 14 and Eq. 15 either only odd-Legendre functions or only even-Legendre functions, according to the parity of the degree ℓ , i.e. the degree of the mode without a magnetic field. As we put $nl = 36$, we have then, 18 terms in the series Eq. 14-15.

3. Results

3.1. The model

The results presented in this paper have been calculated with the following stellar model

Model	M/M_\odot	R/R_\odot	$\log L/L_\odot$	X_c
	1.8	1.531	1.029	0.70

L is the luminosity of the star and X_c the hydrogen fraction at the center. This model has been obtained using usual assumptions for stellar structure and also neglecting all the processes of chemical diffusion.

We found for the non-magnetic acoustic cut-off frequency (assuming an isothermal atmosphere)

$$\nu_{ac,0} = \frac{c_S}{4\pi H} = 2726.27 \mu\text{Hz}. \quad (19)$$

ν denotes the cyclic frequency. Hereafter, we will consider only high frequencies, i.e. from about 1200 μHz to about 2300 μHz , which represent a typical range of observable frequencies (i.e. radial numbers from about 12 to 24).

3.2. The magnetic shift of frequencies

The calculations show that the magnetic field leads to a shift of the real part of the frequency, denoted by $\Delta\nu_R$, and also creates a positive complex component ν_I . The imaginary part comes from the coupling between p-modes and the magnetic field inside the boundary layer. A part of the p-mode's energy is then converted into Alfvénic waves inside this layer, which are dissipated beneath this layer, in the interior (see for instance Roberts & Soward 1983). Therefore, we can write the frequency in the following form

$$\nu = \nu_0(n, \ell) + \Delta\nu_R(n, \ell, m, B_p) + i \nu_I(n, \ell, m, B_p) \quad (20)$$

with ν_0 the frequency without a magnetic field. In the asymptotic limit (for large n) the non-magnetic frequency is related to the radial order by

$$\nu_0(n, \ell) \approx \Delta\nu_0 \left(n + \frac{\ell}{2} + \epsilon\right) \quad (21)$$

with n the radial order and ϵ a constant of the stellar model.

The large separation $\Delta\nu_0$ is

$$\Delta\nu_0 = \left\{ 2 \int_0^R \frac{dr}{c_S(r)} \right\}^{-1} \approx 87.2 \mu\text{Hz}. \quad (22)$$

The results are presented in Fig. 2-5. We note that the effect of the magnetic field, i.e. the frequency shift, increases with the

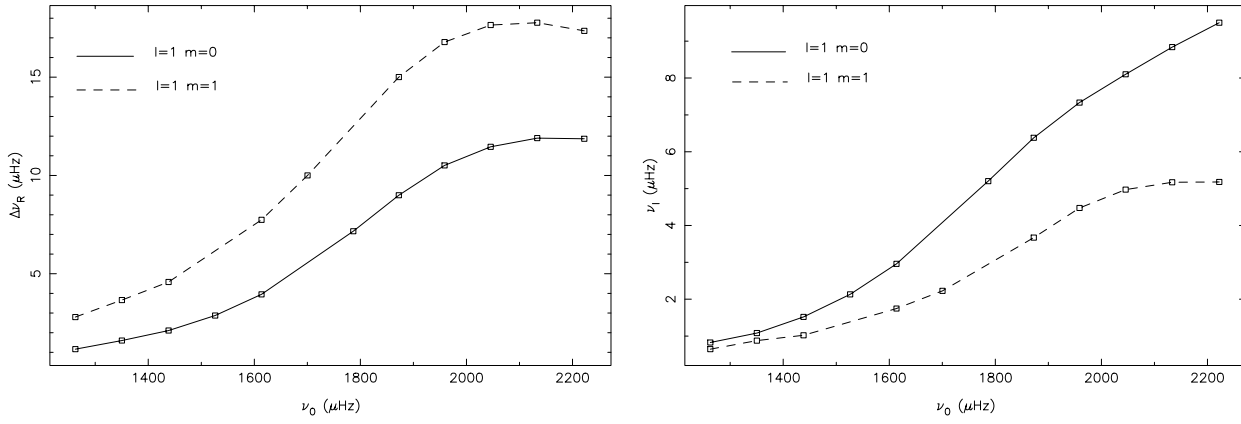


Fig. 3. Shift of the real part of the frequency ($\text{Re}(\nu)-\nu_0$) (left) and the imaginary part (right) as functions of the non-magnetic frequency ν_0 , for a given degree $\ell = 1$, and its corresponding values of m , here $m = 0$ and $m = 1$. These two curves are plotted for a 0.8 kG magnetic field.

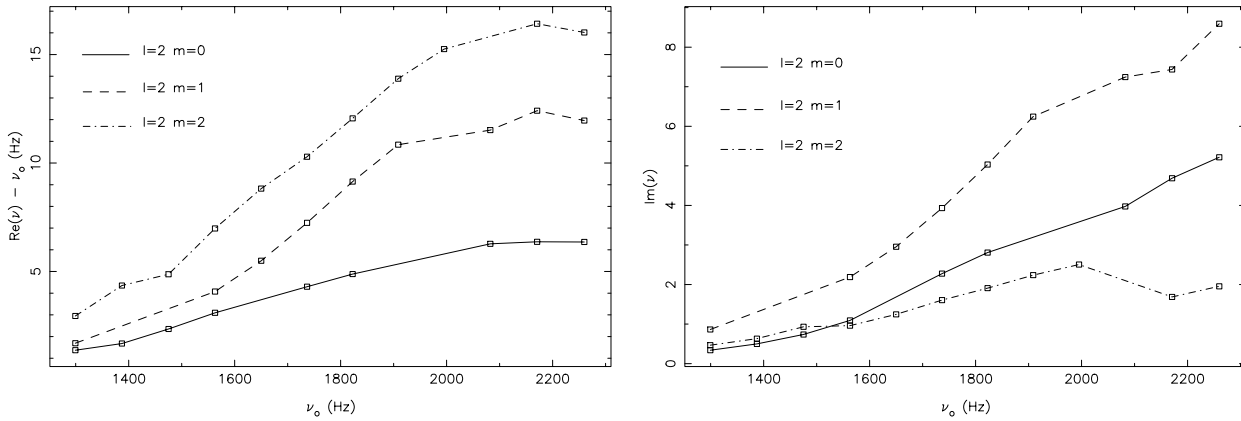


Fig. 4. Shift of the real part of the frequency (left) and the imaginary part (right) for a given degree $\ell = 2$, but for different values of m : $m = 0$, 1 and 2. These curves are plotted for a 0.7 kG magnetic field.

radial order n , for both the real and imaginary parts. This is explained by the fact that the effect of the perturbation, far from the outer turning point, is small. Only modes which have frequencies close to the critical cut-off frequency are significantly affected by the magnetic field.

However, the results we have obtained point out that this shift of frequencies strongly depends on the geometry of the mode, say the value of ℓ and m which corresponds to the geometric dependence of the Lorentz force in θ and m , see Eq. 6-8.

The m -dependence of the frequencies is a direct effect of the magnetic field since it breaks the spherical symmetry of the problem (if we neglect the rotation). It leads then to a raising of the $(2\ell + 1)$ degeneracy of the frequencies (see, for example, Eq. 21). This effect is analogous to the Zeemann effect in Quantum Mechanics. However, it remains a partial degeneracy¹ since the frequencies only depend on the absolute value of m ,

¹ the degeneracy in m is partially lifted because of the axisymmetry of the dipolar magnetic field: there is no difference between waves moving with the phase velocity $v_\phi = \omega_{nlm}/|m|$ and $v_\phi = -\omega_{nlm}/|m|$ in the \vec{e}_ϕ direction; they are affected in the same way by \vec{B}_0 . Therefore, it remains a partial degeneracy for the frequency which just depends on $|m|$.

because the unperturbed magnetic field is dipolar and, therefore, does not depend on the longitude (see Eq. 2).

First, we have investigated the influence of the degree ℓ in the case of axisymmetric oscillations $m = 0$, in Fig. 2. In that case, the typical range of $\Delta\nu_R$ is about $5 - 18 \mu\text{Hz}$ for high overtones, say $\nu \geq 2000 \mu\text{Hz}$ and $2 - 10 \mu\text{Hz}$ for ν_I . We find here the same order of magnitude as Dziembowski & Goode (1996) for axisymmetric oscillations but for a younger star's model.

For both the real and imaginary parts, we see a systematic difference between radial ($\ell = 0$) and non-radial modes ($\ell \neq 0$); for large frequencies the shift in the real part $\Delta\nu_R$ is lower than in the radial case, whereas the shift of the imaginary part is larger, for any value of $\ell \neq 0$ (and for $\nu \geq 1800 \mu\text{Hz}$).

We have investigated how the magnetic effects on oscillations depend on the value of m . The results are presented in Fig. 3-5 for different values of ℓ and in each case for its corresponding values of m ($m \leq \ell$). Let us first examine the shift of the real part $\Delta\nu_R$. As a general result, non-axisymmetric oscillations have greater real shifts of frequency than the case $m = 0$. More, one sees that for any value of ℓ , $\Delta\nu_R$ always increases with m . The modification of the frequency from the axisymmetric case is relatively important. For example, in Fig. 5, we

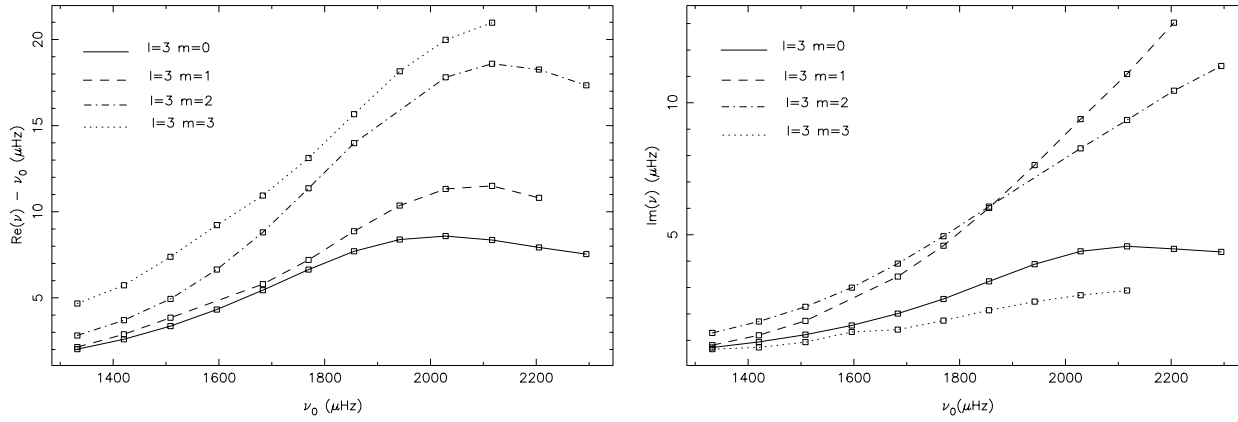


Fig. 5. Shift of the real part of the frequency (left) and its imaginary part (right) for a given degree $\ell = 3$, but for different values of m : $m = 0, 1, 2$ and $\ell = 3$. These curves are plotted for a 0.8 kG magnetic field.

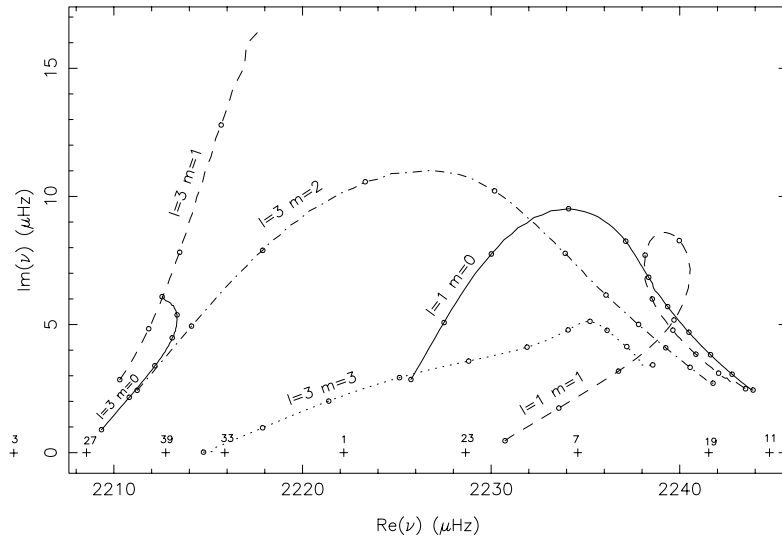


Fig. 6. The imaginary part ($\text{Im } \nu$) of the frequency is plotted as function of the real part ($\text{Re } \nu$), for magnetic fields between 0.5 to 1.5 kG. The points on the curves are spaced by 0.1 kG. Two radial orders ($n = 24$ for $\ell = 3$, and $n = 25$ for $\ell = 1$) are presented. The frequencies in the non-magnetic cases are represented by the crosses (the number above them are the corresponding degrees).

note that $\Delta\nu_R$ which was about $10 \mu\text{Hz}$ for $m = 0$ increases up to $18 \mu\text{Hz}$ in the case $m = 1$, for $B_p = 0.8 \text{ kG}$.

We see, in Fig. 3-5, that the imaginary part, also depends on the value of m . One notes that sectoral modes $\ell = m$, have smaller imaginary parts than axisymmetric modes, whereas modes with $\ell \neq m$ have larger shifts. The amplitude of the modifications introduced for non-axisymmetric oscillations, as for the real part, is also important. As we can see, for $B_p = 0.8 \text{ kG}$ in Fig. 5, ν_I decreases from $4 \mu\text{Hz}$ (for $\nu \approx 2000 \mu\text{Hz}$) in the case $m = 0$ to about $2.5 \mu\text{Hz}$ for $m = 3$ and increases up to $\sim 11 \mu\text{Hz}$ in the case of $m = 1$, say more than twice the value of the axisymmetric case.

These results show that the geometry and the stability of non-axisymmetric oscillations are greatly influenced by the magnetic field. As a matter of fact, the imaginary part introduced by magnetic processes is of the same order as the one due to non-adiabatic effects (see for instance Dziembowski & Goode 1996).

On Fig. 6 and Fig. 7 we plot the imaginary part of the frequency as a function of the real part, for several values of the magnetic fields B_p .

We see again that the behaviour of the frequencies with the magnetic field strongly depends on the geometrical nature of modes. For these graphs we extend the calculations up to 1.5 kG. We see that the damping of modes, i.e. ν_I , passes through a maximum. This maximum is obtained for a particular $B_p = B_{crit}$ whose value depends on the parameters ℓ, m (e.g. for $\ell = 1$ $m = 0$ $B_{crit} \approx 0.8 \text{ kG}$). Such results have already been found by Dziembowski & Goode (1996) but for axisymmetric modes. Note also the behaviour of the mode such as $\ell = m = 1$, whose frequencies form a loop, due to the fact that for some magnetic fields (0.9 – 1.1 kG) both $\Delta\nu_R$ and ν_I decrease.

The observed oscillations are interpreted in terms of the oblique pulsator model (see Kurtz 1982, and later improvements by Dziembowski & Goode 1985, 1986; Kurtz & Shibahashi 1986; Shibahashi & Takata 1993) which states that the pulsation axis is nearly aligned with the magnetic axis and oblique with the rotation axis. According to oblique pulsator model, the observed modes have, generally, a dipole geometry ($\ell = 1$ $m = 0$). Our calculations do not explain this preference since their geometries do not minimize energy losses due to Alfvénic waves. As a matter of fact, we see in Fig. 3 and 6 that in most

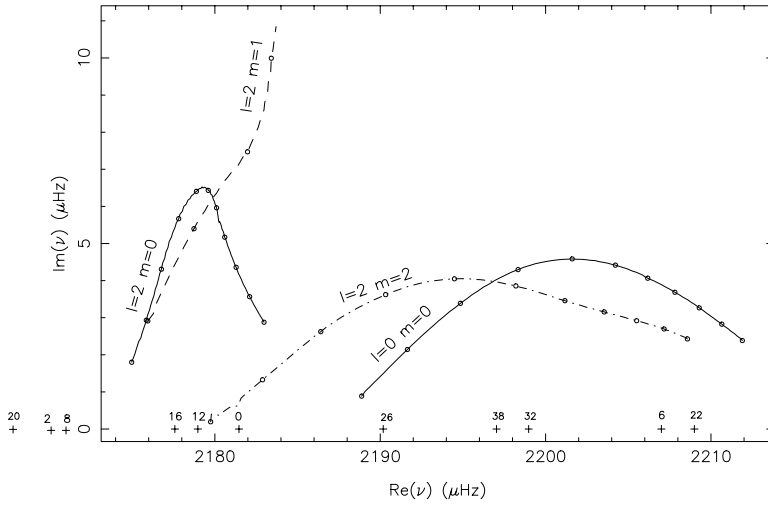


Fig. 7. The imaginary part ($\text{Im } \nu$) of the frequency is plotted as function of the real part ($\text{Re } \nu$), for magnetic fields between 0.5 to 1.5 kG. The points on the curves are spaced by 0.1 kG. Two radial orders ($n = 24$ for $\ell = 2$, and $n = 25$ for $\ell = 0$) are presented. The frequencies in the non-magnetic cases are represented by the crosses (the number above them are the corresponding degrees).

of the cases the imaginary part is generally smaller for $\ell = 1$ $m = 1$ than for the sectoral mode $\ell = 1$ $m = 0$. The same is largely true for other degrees.

3.3. Small separations

As we have seen in the previous sections, the real part of the frequency is shifted up to $20 \mu\text{Hz}$. This value is of the same order as the small separations in the non-magnetic limit, say

$$S_{\ell,n} = \nu_{\ell,n+1} - \nu_{\ell+2,n}. \quad (23)$$

These separations, in the non-magnetic case, are widely influenced by the deep stellar interior. Consequently, they give useful information about these regions and therefore an estimation of the stellar age.

We see that the changes due to deep stellar structure (in the non-magnetic case) are of the same order as the magnetic shifts of frequencies ($\sim 15 - 20 \mu\text{Hz}$). The non-magnetic separations are degenerate in m , as the corresponding frequencies. However, the magnetic field raises partially the degeneracy for ν and, therefore, the degeneracy for S . This implies that the small separations in the case of non-axisymmetric oscillations with magnetic field depend on the azimuthal degree m . Let us define this separation by

$$S_{\ell,n}^{mm'} = \nu_{\ell,n+1}^m - \nu_{\ell+2,n}^{m'}. \quad (24)$$

An example of this separation is given in Fig. 8, for $\ell = 0$, $\ell = 2$ and $\ell = 1$, $\ell = 3$.

We note, in these graphs, that the small separations do not have the same behaviour with the magnetic field, depending on the mode's geometry. In the case of even degrees ($\ell = 0$, $\ell = 2$) the small separations with $m' \neq 0$ are smaller than the axisymmetric case and decrease with m' . In the case of odd degrees ($\ell = 1$, $\ell = 3$) we see that $S_{1,19}^{0m'} < S_{1,19}^{1,m'}$ with $m' = 0, 1, 2, 3$. More, one can note that for a given value of m (i.e. 0 or 1) the small separations decrease with the value of m' .

These results show that it is very complicated to get information on stellar structure in terms of these small separations, because of the perturbations introduced by the magnetic field.

3.4. Angular geometry of modes

In this subsection we discuss the influence of the angular dependence of the Lorentz force on the geometry of p-modes oscillations. As we have seen in the previous subsection, the boundary condition for p-modes $\mathcal{F}(\theta, \omega, m)$ depends on θ which is a direct consequence of the θ -dependence of \vec{L} . We cannot represent a mode in the interior by a single spherical harmonic, as for non-magnetic oscillations, but we need to expand the solutions y_p, q_p as a series of associated Legendre functions, Eq. 14 and Eq. 15. We saw that this angular expansion involved only functions which have the same parity for ℓ and the same value of m .

The calculations show that, when B_p increases, the number of terms with a significant amplitude in the series increases and the “weight” of these terms, say the value of $D_{k,m}$, changes.

The contribution of these terms is found in the energy of the mode. The kinetic energy $e_{l,m}$ of a mode can be written as

$$e_{l,m} = \frac{\omega_R^2}{4} \int_{V_{\text{fit}}} \left| \xi_{l,m}^{\rightarrow} \right|^2 \rho dV \quad (25)$$

with the displacement, $\xi_{l,m}^{\rightarrow} = \sum_k D_{km} \xi_{k,m}^{\rightarrow}$ and in spherical coordinates

$$\xi_{k,m}^{\rightarrow} = r \left(y_k(r), y_{h,k}(r) \frac{\partial}{\partial \theta}, \frac{y_{h,k}(r)}{\sin \theta} \frac{\partial}{\partial \phi} \right) Y_k^m(\theta, \phi) e^{i\omega t} \quad (26)$$

$$y_{h,k} = \frac{1}{r^2 \rho_0 \omega^2} (p_0(q_k(r) + y_k(r)V) + \rho_0 \Phi_{1k}) \quad (27)$$

where Φ_1 represent the Eulerian perturbation of the gravitational potential.

Since P_k^m form an orthogonal basis, we have

$$e_{l,m} = \sum_k e_{k,m} \quad (28)$$

with,

$$e_{k,m} = \frac{\omega_R^2}{4} |D_{km}|^2 \mathcal{I}_k \langle \rho \rangle R^5 \quad (29)$$

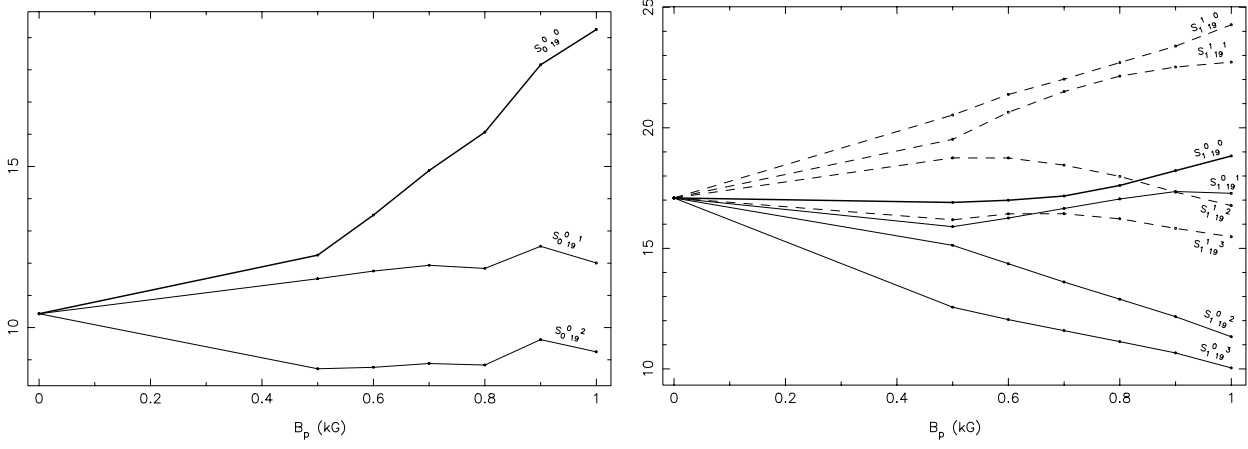


Fig. 8. (left) Small separations (in μHz) $S_{0,19}^m = \nu_{0,20} - \nu_{2,19}^m$ for $m = 0, 1, 2$ as function of the photospheric magnetic field. (right) Small separations $S_{1,19}^{mm'} = \nu_{1,20}^m - \nu_{3,19}^{m'}$ for $m = 0, 1$ $m' = 0, 1, 2, 3$. The dashed curves corresponds to $m = 0$ and $m' = 0, 1, 2, 3$ and the full curves corresponds to $m = 1$ and $m' = 0, 1, 2, 3$. In both cases the heavy line is for the axisymmetric case.

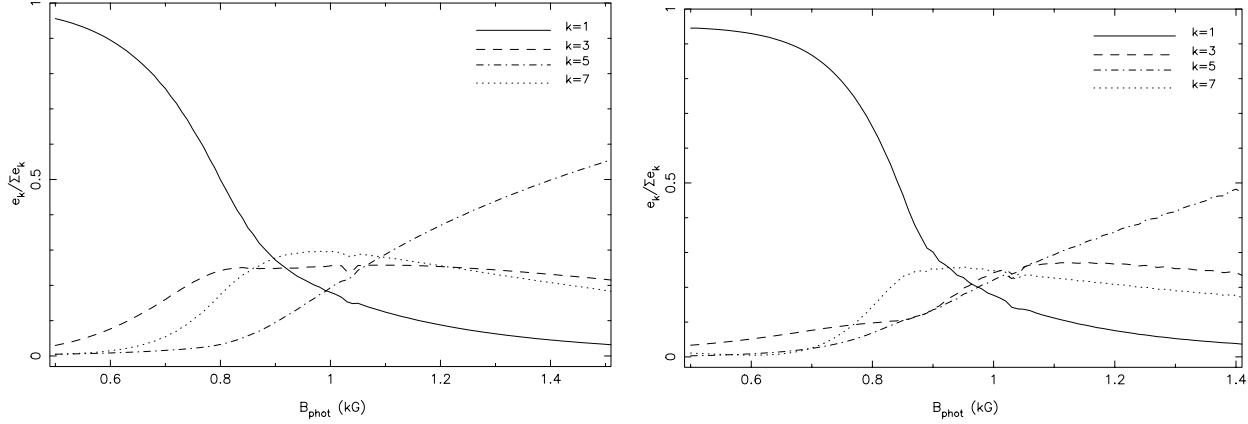


Fig. 9. We represent in the ordinate the ratio of the mode's energy e_k , for $\ell = 1$ $m = 0$ (left) and $\ell = 1$ $m = 1$ (right), divided by the total energy $\sum_k e_k$, as function of magnetic field. The expression of this ratio is given in the text.

$$\mathcal{I}_k = \int_0^{x^{\text{fit}}} x^4 \frac{U}{c_1} (|y_k|^2 + k(k+1)|y_{h,k}|^2) dx \quad (30)$$

with

$$U = \frac{d \ln M_r}{d \ln r} \quad c_1 = 3x^3 \frac{M}{M_r}. \quad (31)$$

$\langle \rho \rangle$ is the mean density of the star. In order to represent the weight of each component of the total energy of the mode, we plot the following ratio

$$\eta_{k,m} = \frac{e_{k,m}}{e_{l,m}} = \frac{|D_{km}|^2 \mathcal{I}_k}{\sum_k |D_{km}|^2 \mathcal{I}_k}. \quad (32)$$

Several plots of η_k are given in Fig. 9-13, as function of the magnetic field. We plot only the components k which have non negligible amplitudes. We see clearly that the energy of the main component of the mode decreases when B_p increases, whereas the energy of new components increases.

Let us examine, for example, the case of $\ell = 1$ in Fig. 9. We see that when B_p is relatively small, ≤ 0.6 kG, about 100% of the energy is contained in the component $k = 1$, $m = 1$.

However, the components $k = 3, 7$ get non negligible amplitudes when $B_p \sim 0.7 - 0.8$ kG. And for $B_p = 0.89$ kG the energies of the three components $k = 1, 3, 7$ are equal, each of them has about 30% of the total energy of the mode $\ell = 1$ $m = 1$. Nonetheless, the component $k = 5$ also increases with the magnetic field and becomes dominant for $B_p \geq 1.1$ kG. We see that the presence of another component depends on the value of m ; see for example the case of $\ell = 2$ $m = 1$ and $m = 2$ in Fig. 13. The values of the degrees, involved in this mixing, strongly depend on m ; the case $m = 1$ has larger degrees for the Legendre functions than the case $m = 2$. One realizes that the identification of modes is very difficult in the presence of a strong magnetic field because the dominant component, and then its geometry, of a given mode depends on the magnetic field. In the present case, for $B_p \leq 0.9$ kG the dominant component is $k = 1$ and for $B_p \geq 1.1$ it is $k = 5$. The magnetic field totally changes the geometrical nature of the mode. One can note that for magnetic fields above 1.1 kG the mode $\ell = 1$, $m = 0$ or $m = 1$ becomes undetectable for observers because the spatial averaging of the component $k = 5$ vanishes.

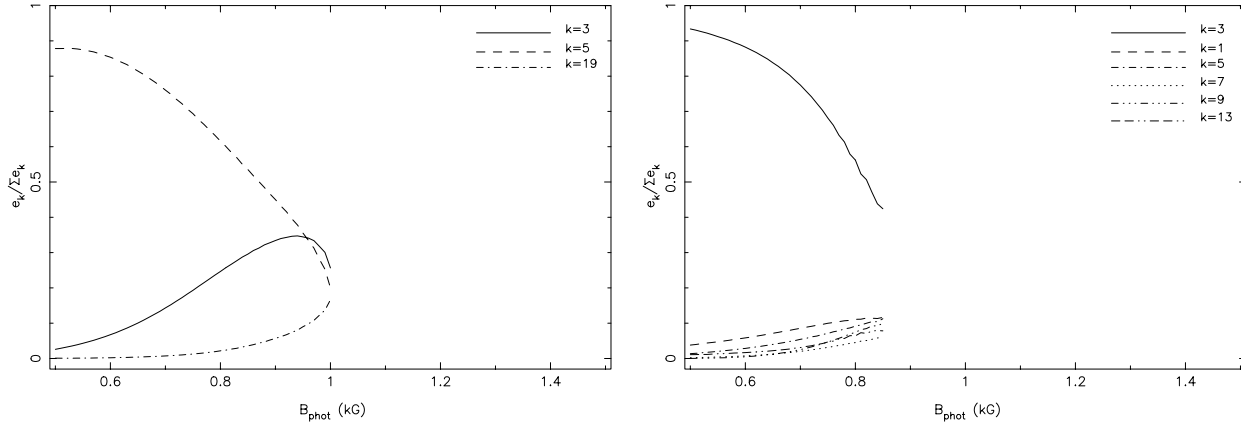


Fig. 10. The same ratio η_k for $\ell = 3$ $m = 0$ (left) and $\ell = 3$ $m = 1$ (right) as function of magnetic field.

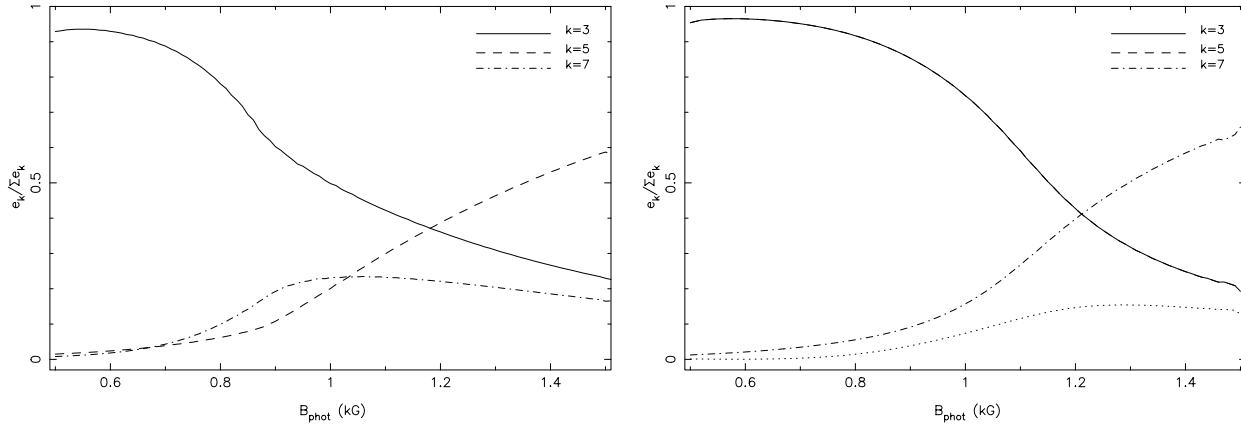


Fig. 11. The same ratio η_k for $\ell = 3$ $m = 2$ (left) and $\ell = 3$ $m = 3$ (right) as function of magnetic field.

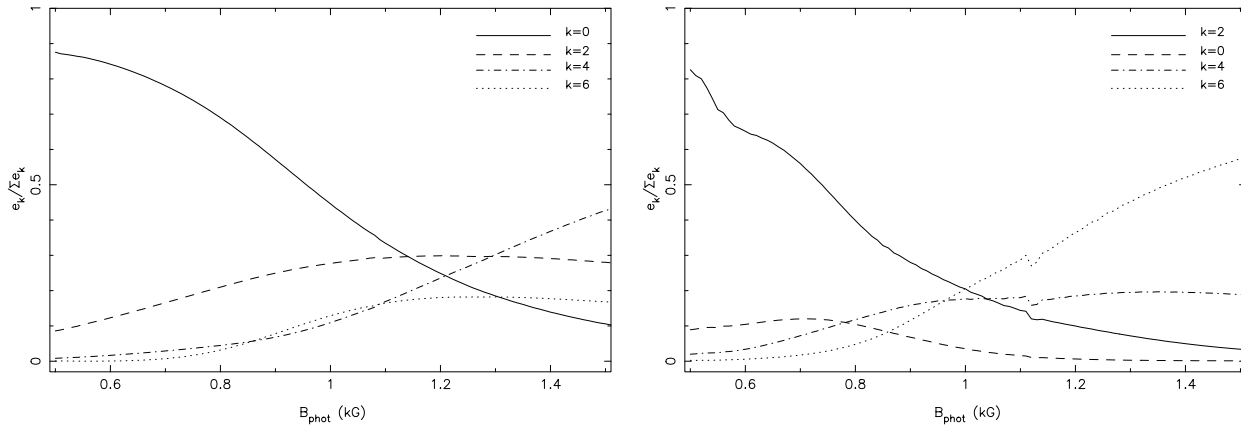


Fig. 12. The same figure as the previous one but for $\ell = 0$ (left) and $\ell = 2$ $m = 0$ (right).

To the contrary, we can expect to see modes which are invisible without a magnetic field, say with $\ell \geq 4$, but for which in the case of strong B_p the dominant component is obtained for $k \leq 3$. This is the case of $\ell = 5$, $m = 1$ as we can see on Fig. 14. However, we should note that one cannot arbitrarily increase the magnetic field because of the main assumption we made for the magnetic layer, i.e. the plane parallel approximation. To be valid the magnetic layer must be situated close to the top of the star.

When B_p increases, the base of the boundary layer has to be deeper (say for greater densities) in the star in order the ratio β (see Eq. 1) remains small to insure the decoupling between acoustic and Alfvénic modes. We give in Table 1 in Appendix A several positions of x_{fit} for different values of B_p .

We also assumed small horizontal wave numbers in the magnetic layer compared with the radial ones. This assumption still remains valid if the degree of Legendre function is not too large.

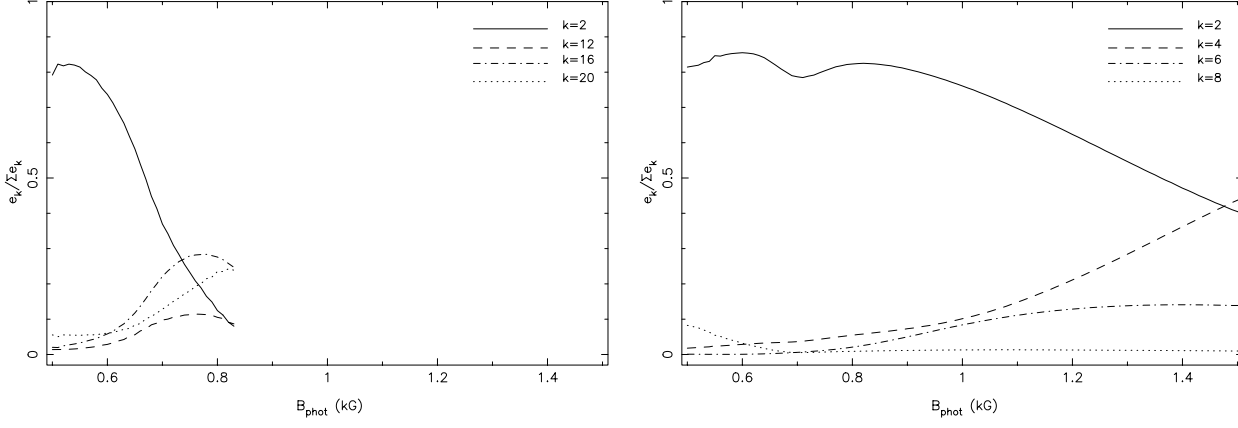


Fig. 13. The same figure as the previous one but for $\ell = 2, m = 1$ (left) and $\ell = 2, m = 2$ (right).

As the series Eq. 14 and Eq. 15 require higher orders when the magnetic field increases, we have a limitation on the value of B_p . In our case, the plots of η_k show that even in the case of magnetic fields above 1 kG the maximal amplitude is for small degrees of Legendre functions, i.e. ≤ 10 , except for $\ell = 2, m = 1$ and $\ell = 3, m = 0$ and $m = 1$ for which some polynomials of large degrees have strong components in the expansions Eq. 14,15. For the cases of $\ell = 3, m = 0$ and $\ell = 2, m = 1$ we stop the calculations for $B_p = 1.0$ kG and $B_p = 0.83$ kG, respectively, because they involve degrees larger than 20 for higher magnetic fields, and then are incompatible with the assumptions we made.

3.5. Contribution to pulsational damping

From the system of linearized equations Eq. A.1-A.4 in appendix A, one can derive an equation for energy conservation (by multiplying with the complex conjugate of ξ and integrating over a given volume \mathcal{V})

$$\begin{aligned}
 \omega^2 \int_M \left| \vec{\xi} \right|^2 \rho dV = & \oint_S \left\{ \left(\delta p - \vec{\xi} \cdot \vec{\nabla} p_0 + \rho_0 \Phi_1 \right) \vec{\xi}^* \right\} \cdot \vec{dS} \\
 & - \oint_S \left\{ 1/4\pi \left(\vec{B}_0 \wedge \vec{\xi}^* \right) \wedge \vec{B}_1 \right\} \cdot \vec{dS} \\
 & + \int_{\mathcal{V}} \left\{ \frac{|\delta p|^2}{\Gamma_1 p_0} + \vec{\xi} \cdot \vec{\nabla} \ln \rho_0 \vec{\xi}^* \cdot \vec{\nabla} p_0 \right\} dV \\
 & + \int_{\mathcal{V}} \left\{ \rho_0 \Phi_1 \left(\frac{\delta p^*}{\Gamma_1 p_0} - \vec{\xi}^* \cdot \vec{\nabla} \ln \rho_0 \right) \right\} dV \\
 & - \int_{\mathcal{V}} \left\{ 2Re \left(\frac{\delta p^*}{\Gamma_1 p_0} \vec{\xi} \cdot \vec{\nabla} p_0 \right) + \frac{|B_1|^2}{4\pi} \right\} dV. \quad (33)
 \end{aligned}$$

This formula is useful for two reasons. First, it provides a way to estimate the numerical precision of the frequencies (see in Appendix C). Second, it can be used to find the angular location of the damping zone. To do this, we take the imaginary part of Eq. 33 and neglect the contribution of the magnetic field since,

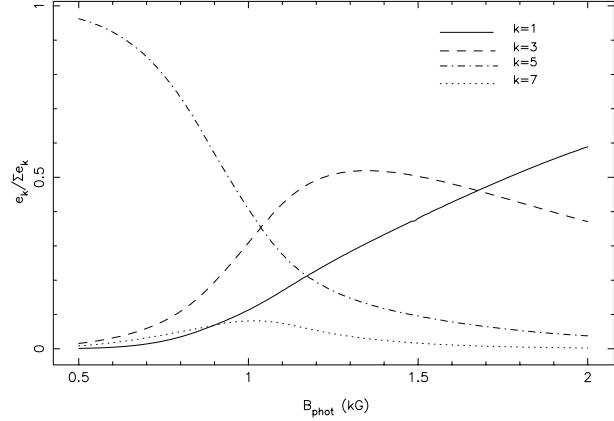


Fig. 14. Ratio of the mode's energy e_k for $\ell = 5, m = 1$ divided by the total energy $\sum_k e_k$, as function of magnetic field. We see that for $B_p \geq 1.7$ kG this mode $\ell = 5$ becomes detectable because its main component is $k = 1, m = 1$

at r_{fit} we have $\beta \ll 1$. Then, we get

$$\begin{aligned}
 2\omega_R \omega_I \int_{M_{\text{fit}}} \left| \vec{\xi} \right|^2 dm = & Im \oint_{S_{\text{fit}}} \left(\delta p + \rho_0 \Phi_1 \right) \xi_r^* dS \\
 & + Im \int_{M_{\text{fit}}} \Phi_1 \left(\frac{\delta p^*}{\Gamma_1 p_0} - \xi_r^* \frac{\partial \ln \rho_0}{\partial r} \right) dm.
 \end{aligned}$$

Neglecting the effect of the gravitational potential which is small for high frequencies, one can write the imaginary part of the frequency as

$$\omega_I = \int Im \{ g(r_{\text{fit}}, \cos \theta) \} d(\cos \theta) \quad (34)$$

with,

$$g(r_{\text{fit}}, \cos \theta) = \frac{\pi r_{\text{fit}}^3}{\omega_R} \frac{p_0 q y^*}{\int_{M_{\text{fit}}} \left| \vec{\xi} \right|^2 dm}. \quad (35)$$

Then, one sees that the imaginary part of frequency comes from the imaginary part of the acoustic flux $\delta p \xi_r^*$ through the

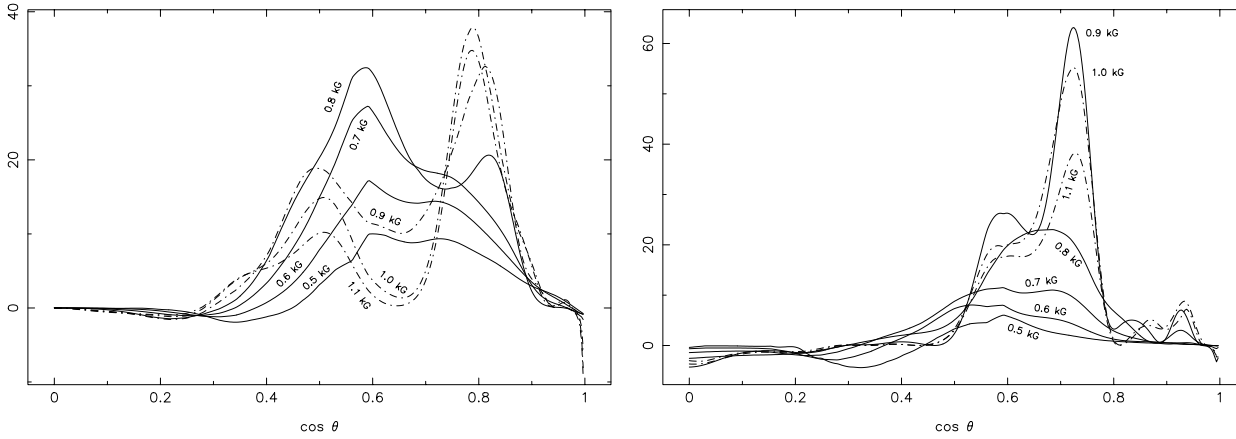


Fig. 15. Plots of the imaginary part of the function $g(r_{\text{fit}}, \cos \theta)$ for different magnetic fields (0.5 – 1.1 kG) for two modes $\ell = 1, m = 0$ (left) and $\ell = 1, m = 1$ (right) corresponding to the modes in Fig. 6. The full curves correspond to an increasing ω_I with B_p whereas the dot-dashed curves correspond to a decay of ω_I with B_p .

fitting surface. $g(r_{\text{fit}}, \cos \theta)$ corresponds to this flux normalized by the inertia of the mode. One can verify in Fig. 15 that $\text{Im}\{g(r_{\text{fit}}, \cos \theta)\}$, first, depends on θ , but its contribution to ω_I comes from a region located essentially between $\cos \theta \approx 0.4$ and the magnetic pole $\cos \theta = 1$. The location of the maximum of this function $\text{Im}\{g(r_{\text{fit}}, \cos \theta)\}$ depends on the value of B_p : one sees in Fig. 15 (a) that the maximum is for $\cos \theta \approx 0.6$ for $B_p \leq 0.8$ kG, i.e. for $\cos \theta_0$ defined in Sect. 2.1, whereas for $B_p \geq 0.9$ kG the maximum is for $\cos \theta \approx 0.85$ which corresponds to an extremum of the Legendre polynomial P_5^0 . We find again that the presence of the mixing of spherical harmonics described in Sect. 3.4. One can check in Fig. 9 that the Legendre polynomial of degree 5 starts to dominate the angular geometry of the mode $\ell = 1, m = 0$ from $B_p \approx 1.1$ kG. Note that even in the case of $B_p = 0.8$ kG (full line) one sees the contribution of P_5^0 with the second extremum of $g(r_{\text{fit}}, \cos \theta)$ close to $\cos \theta = 0.85$.

One sees that the integral of the function g decreases from $B_p = 0.8$ kG which leads to a decay of ω_I , which corresponds to the Fig. 6. For the case of the non-axisymmetric mode $\ell = 1, m = 1$, we find the same kind of results, except that for $B_p \geq 0.9$ kG the maximum of the function g is for $\cos \theta \approx 0.75$.

4. Conclusion and discussion

We have investigated the influence of a strong magnetic field on stellar oscillations in the case of Ap stars. With our model of $M = 1.8M_\odot$, $R = 1.5M_\odot$ and $X_c = 0.7$, we find that for B_p smaller than 0.8-0.9 kG the magnetic field has a damping effect on p-modes oscillations which increases with B_p , whereas above 0.9 kG this damping effect decreases with B_p . The real part of ν is shifted up to $20 \mu\text{Hz}$ from its non-magnetic value. The imaginary part which comes from Alfvénic wave losses, produced in the magnetic layer, has values up to $15 \mu\text{Hz}$. Moreover, these results depend on the geometry of the mode, particularly on the azimuthal degree m . The degeneracy of frequencies is, then, partially raised by the magnetic field. The real part, for non-axisymmetric oscillations, increases with m and is always

greater than for the case $m = 0$. The imaginary parts are greater than in the axisymmetric frequencies, except for sectoral modes which are less damped than in the axisymmetric case.

We also showed that the magnetic field complicates the identification of modes, especially when the value of B_p becomes of the order of 0.8 – 1.0 kG, because of the angular mixing of solutions in the interior. This effect also depends on the value of m .

The aim of this work was to show the modifications of frequencies due to a strong magnetic field. That's why we used a very simple stellar model of oscillations, neglecting other important processes in those stars such as non-adiabatic processes and the effect of chemical diffusion. The computation of more realistic frequencies needs to take into account these effects.

In this paper we have considered the direct effect of the magnetic field on the oscillations. It cannot, however, explain the observed preference for dipole modes ($\ell = 1, m = 0$) in roAp stars, since, in the case of our calculations and hypothesis, they do not minimize energy losses due to Alfvénic waves. Thus, the explanation of mode selection remains a challenge to theory. Another piece of observational evidence is that chemical diffusion occurs in Ap stars. The idea that chemical spots play a role in the selection is not new (see Dolez et al. 1988). To this effect to work we postulate that there is hydrogen in excess in the polar region. This is different from that in Dolez et al. (1988) because they expected mostly Helium driving. However, it has been shown by Dziembowski & Goode (1996) and Gautschy et al. (1998) that only the kappa-mechanism in the hydrogen ionisation zone can explain high frequencies excitation in roAp stars. Therefore, p-modes could be more excited at the pole than at the equator. This configuration could explain that modes are aligned with the magnetic axis.

Appendix A:

The aim of this appendix is to explain in a detailed way how to obtain the boundary condition $\mathcal{F}(\theta, \omega, m)$.

A.1. Set of equations

The full set of linearized ideal MHD equations in the case of adiabatic oscillations is

— the equation of motion

$$-\rho_0\omega^2 \vec{\xi} = -\vec{\nabla} P_1 + \rho_1 \vec{g}_0 + \frac{\vec{\nabla} \wedge \vec{B}_1}{4\pi} \wedge \vec{B}_0 \quad (\text{A.1})$$

— the conservation of mass

$$\rho_1 = -\vec{\nabla} \cdot (\rho_0 \vec{\xi}) \quad (\text{A.2})$$

— the adiabatic condition

$$\frac{\delta p}{p_0} = \Gamma_1 \frac{\delta \rho}{\rho_0} \quad (\text{A.3})$$

— the equation of induction

$$\vec{B}_1 = \vec{\nabla} \wedge (\vec{\xi} \wedge \vec{B}_0) \quad (\text{A.4})$$

where the quantities P_1 , ρ_1 , \vec{B}_1 denote the Eulerian perturbations of the pressure, density and the magnetic field, and δp , $\delta \rho$ denote the Lagrangian perturbation of the pressure and the density. The temporal dependence is assumed to be $\sim e^{i\omega t}$. The displacement $\vec{\xi}$ and the Lagrangian perturbation of pressure are given by Eq. 3 and Eq. 4. As we consider high frequencies, we adopt the Cowling approximation, i.e. we neglected the perturbation of the gravitational potential, $\vec{g}_1 = \vec{0}$.

In order to simplify this system of equations, we have made several assumptions. First, we assumed large radial wave numbers, therefore,

$$\frac{\partial X}{\partial x} \gg X \quad (\text{A.5})$$

where X is any perturbed quantity. More, we suppose that horizontal wave numbers are small compared with radial wave numbers, ie

$$\frac{\partial X}{\partial x} \gg \frac{\partial X}{\partial \theta}. \quad (\text{A.6})$$

We also assumed $x \approx 1$. The result for the Lorentz force with these approximations is given by Eq. 6-8. After simplifications thanks to the previous assumptions and a little algebra, we get the following system

$$\frac{dy}{dx} = -\frac{q}{\Gamma_1} - \frac{\tilde{w}}{\sin^2 \theta} \quad (\text{A.7})$$

$$\frac{dq}{dx} = V \left\{ \frac{\tilde{w}}{\sin^2 \theta} + q + c_1 \sigma^2 \left(y \left(1 + \frac{\tan^2 \theta}{4} \right) - \frac{h}{2 \cos^2 \theta} \right) \right\} \quad (\text{A.8})$$

$$\frac{dh}{dx} = \tilde{f} - \frac{\tilde{w}}{2} \quad (\text{A.9})$$

$$\frac{d\tilde{f}}{dx} = \frac{c_1 \alpha \sigma^2}{3 \cos^2 \theta} \left(y \frac{\sin^2 \theta}{2} - h \right) \quad (\text{A.10})$$

$$\frac{d\tilde{w}}{dx} = \tilde{g} + \frac{m^2 h}{2 \cos^2 \theta} \quad (\text{A.11})$$

$$\frac{d\tilde{g}}{dx} = \frac{c_1 \alpha \sigma^2}{3 \cos^2 \theta} \left(-\tilde{w} - \frac{m^2}{c_1 V \sigma^2} (q + yV) \right) \quad (\text{A.12})$$

A.7 is the equation of continuity, A.8 the equation of motion on \vec{e}_r , A.10 the equation of motion on \vec{e}_θ , A.12 the equation of motion on \vec{e}_ϕ . A.9, A.11 have been introduced to get a system of differential equations of the first order.

The following variables have been introduced

$$h = y \frac{\sin^2 \theta}{2} - z \cos \theta \sin \theta \quad (\text{A.13})$$

$$\tilde{w} = im \sin \theta w \quad (\text{A.14})$$

and

$$\alpha = \frac{12\pi GM}{B_p^2 R} \rho_0 = \frac{3V}{\beta \Gamma_1} \quad (\text{A.15})$$

with β defined by Eq. 1.

V and c_1 are defined by

$$V = -\frac{d \ln p}{d \ln r} = \frac{\rho_0 g_0 r}{p_0} \quad c_1 = 3x^3 \frac{M}{M_r}. \quad (\text{A.16})$$

We also introduced the dimensionless frequency σ by

$$\omega^2 = 3 \frac{GM}{R^3} \sigma^2 \quad (\text{A.17})$$

with the range of frequencies we consider in this paper [1200,2300] μHz , it corresponds to a range of [10,19] for σ .

We see that the system Eq. A.7-A.12 is singular at the pole and the equator. These two limit cases needs a special treatment (see Appendix B)

The upper and lower boundaries of the magnetic layer depend, as expected, on the value of the photospheric magnetic field B_p . For the top of this layer, we required that \vec{B}_1 tends to vacuum field ($\alpha \rightarrow 0$) as ρ tends to zero. Therefore, we can put the right hand side of Eq. A.10 and Eq. A.12 equal to zero. This requires us to extend the atmosphere sufficiently high to have low density and then verify $\alpha \sigma^2 \ll 1$. At the base of the magnetic layer we need two conditions. The first one corresponds to a negligible magnetic pressure compared with the gas pressure; for this we require $\beta_{\text{fit}} \ll 1$. The second condition concerns Alfvénic waves. We require that their wavelengths are much shorter than the pressure scale height, i.e. $\alpha \sigma^2 \gg V^2$. We give in Table 1 several values of α at the top and the base of the magnetic layer.

The general solution vector $S = (y, q, h, \tilde{f}, \tilde{w}, \tilde{g})$ of this system can be written as a linear combination of six linearly independent solutions. However, we assume that the star is an isolated system, i.e. we reject inward propagating waves which could come from infinity. Hence, this reduces our solutions to three inside the magnetic layer

$$S = C_1 S_1 + C_2 S_2 + C_3 S_3. \quad (\text{A.18})$$

There are two steps in the numerical integration. The first one consists of finding the three peculiar solutions S_i for each radial position x in the magnetic layer. To do this, we start from the top of the layer with analytical peculiar solutions which are found thanks to a local analysis. We then integrate them numerically, with a method of Runge-Kutta, through the magnetic layer to the

Table A.1. Limits of the magnetic boundary layer for different values of the magnetic fields, and in each case, the value of the two parameters α and β describing the importance of the magnetic field.

B_p (kG)	x_{fit}	x_{top}	α_{fit}	α_{top}	β_{fit}	β_{top}
0.5	0.9867	1.00152	$0.989 \cdot 10^5$	$0.183 \cdot 10^{-3}$	$0.478 \cdot 10^{-2}$	$0.107 \cdot 10^6$
1.0	0.9816	1.00123	$0.616 \cdot 10^5$	$0.186 \cdot 10^{-3}$	$0.580 \cdot 10^{-2}$	$0.891 \cdot 10^6$
1.5	0.9773	1.00107	$0.503 \cdot 10^5$	$0.184 \cdot 10^{-3}$	$0.588 \cdot 10^{-2}$	$0.900 \cdot 10^8$
2.0	0.9732	1.00094	$0.454 \cdot 10^5$	$0.188 \cdot 10^{-3}$	$0.557 \cdot 10^{-2}$	$0.877 \cdot 10^8$

base ($x = x_{\text{fit}}$). The next step of the numerical integration is to find the coefficients of the linear combination C_i . This is done at the base of the boundary layer adding another condition. Since at x_{fit} one has $\beta \ll 1$, we assumed a full decoupling between p-modes and Alfvénic modes beneath the magnetic layer. We add also the condition that there are only inwards propagative Alfvénic waves under the magnetic layer (see also Roberts & Soward 1983). Then the solution at the base of the magnetic layer has the following form

$$S = C_p S_p + C_A^1 S_A^1 + C_A^2 S_A^2. \quad (\text{A.19})$$

The Alfvénic solutions $S_A^{1,2}$ are obtained with a WKB method. The components of S_p at the fit only depend on the two variables y_p and q_p . (see below). Therefore, the unknown quantities are $C_1, C_2, C_3, C_A^1, C_A^2$ and C_p which are found matching the solutions Eq. A.18 and Eq. A.19. This leads to a linear homogeneous system of equations which has non trivial solutions if the secular determinant is zero. This condition gives the relation between q_p and y_p at $x = x_{\text{fit}}$, that is to say the boundary condition $\mathcal{F}(\theta, \omega, m)$.

A.2. External boundary conditions

We adopted here a local analysis of the system assuming that the coefficients of the system Eq. A.7-A.12 are constant (we assume to be in an isothermal atmosphere). The solutions have the form e^{kx} . This gives a relation of dispersion

$$k^2(k^2 - Vk + \frac{c_1 \sigma^2}{\Gamma_1} (1 + \frac{\tan^2 \theta}{4})) (k^2 + \frac{m^2}{4 \cos^2 \theta}) = 0. \quad (\text{A.20})$$

One gets three groups of solutions. As said before, we keep only outward propagating or decreasing waves in the atmosphere. The solution may be written as

$$S(\text{top}) = C_1 S_1(\text{top}) + C_2 S_2(\text{top}) + C_3 S_3(\text{top}). \quad (\text{A.21})$$

The three remaining solutions correspond to three different waves numbers of Eq. A.20.

The first one is

$$k_1 = \frac{V}{2} \left(1 - \sqrt{1 - \frac{\sigma^2}{\sigma_{ac,0}^2} (1 + \frac{\tan^2 \theta}{4})} \right) \quad (\text{A.22})$$

$\sigma_{ac,0}$ being the dimensionless non-magnetic acoustic cut-off frequency and is given by

$$\sigma_{ac,0} = \sqrt{\frac{\Gamma_1 V}{4c_1}}. \quad (\text{A.23})$$

The corresponding vector solution can be written as followed

$$S_1(\text{top}) = (1, -\Gamma_1 k_1, 0, 0, 0, 0) \quad (\text{A.24})$$

where we choose the normalization condition $y_1 = 1$. The second type of solution obeys the condition

$$k_2 = 0. \quad (\text{A.25})$$

This gives a second vector (with $h = 1$)

$$S_2(\text{top}) = (2/(3 \cos^2 \theta + 1), 0, 1, 0, 0, -m^2/2 \cos^2 \theta). \quad (\text{A.26})$$

For the last vector corresponding to the wave number

$$k_3 = \frac{-im}{2 |\cos \theta|} \quad (\text{A.27})$$

one can choose with $m \neq 0$ (with $\tilde{\omega} = 1$)

$$S_3(\text{top}) = \left(\frac{-i \cos \theta}{m} \frac{2}{3 \cos^2 \theta + 1}, \frac{\Gamma_1}{3 \cos^2 \theta + 1} - \frac{\Gamma_1}{\sin^2 \theta}, \frac{-i \cos \theta}{m}, 0, 1, 0 \right) \quad (\text{A.28})$$

Next, each component of the vector S is integrated by a method of Runge-Kutta of the fourth order with adapted step size. The result is the values $S_1(\text{fit}), S_2(\text{fit})$ and $S_3(\text{fit})$.

A.3. Inner boundary conditions

To obtain the expression for these coefficients, we require new conditions at the base of the magnetic layer. In this part of the star, the ratio β is very small. This means that the Alfvénic speed is negligible compared with the sound speed. Since the two perturbations of B and p , say the Alfvénic waves and pressure waves are propagating with very different speeds, it appears a decoupling between the two. Mathematically, this decoupling appears in the system Eq. A.7- A.12 because of the small value of $\eta = 1/(\alpha \sigma^2)$. Then, a solution of the system Eq. A.7-A.12 can be written as

$$S(\text{fit}) = C_p S_p + C_A^1 S_A^1 + C_A^2 S_A^2. \quad (\text{A.29})$$

The subscript “ p ” refers to the p-mode solution, whereas the subscript “ A ” corresponds to the Alfvénic solution. Since, the effect of the magnetic field is very small below the magnetic layer, we can again use a perturbative approach to find the solutions.

A.31. p-modes solution

This corresponds to the zeroth-order of perturbation, $\eta = 0$. Then, Eq. A.7-Eq. A.12 reduces to

$$h_p = \frac{\sin^2 \theta}{2} y_p \quad \widetilde{w}_p = -\frac{m^2}{c_1 V \sigma^2} (q_p + y_p V) \quad (\text{A.30})$$

$$\frac{dy_p}{dx} = -\frac{q_p}{\Gamma_1} \quad (\text{A.31})$$

$$\frac{dq_p}{dx} = V \{q_p + c_1 \sigma^2 y_p\} \quad (\text{A.32})$$

where we neglected the terms due to \widetilde{w}_p since they are small compared with y_p and q_p as we can see on Eq. A.30. This system corresponds to the system of equations in the case of non-magnetic and adiabatic radial oscillations (in the Cowling approximation).

we obtain

$$\widetilde{f}_p = -\frac{\sin^2 \theta}{2\Gamma_1} q_p \quad (\text{A.33})$$

$$\widetilde{g}_p = -m^2 \left(\frac{1}{c_1 \sigma^2} \left(1 - \frac{1}{\Gamma_1}\right) q_p + \left(1 + \frac{\tan^2 \theta}{4}\right) y_p \right). \quad (\text{A.34})$$

Then, we can write the vector solution for p-modes as function of y_p and q_p .

$$\begin{aligned} S_p &= \left(y_p; q_p; h_p; \widetilde{f}_p; \widetilde{w}_p; \widetilde{g}_p \right) \\ &= y_p \left(1, 0, \frac{\sin^2 \theta}{2}, 0, \frac{-m^2}{c_1 \sigma^2}, -m^2 \left(1 + \frac{\tan^2 \theta}{4}\right) \right) \\ &+ q_p \left(0, 1, 0, \frac{-\sin^2 \theta}{2\Gamma_1}, \frac{-m^2}{c_1 V \sigma^2}, \frac{-m^2}{c_1 \sigma^2} \left(1 - \frac{1}{\Gamma_1}\right) \right). \end{aligned} \quad (\text{A.35})$$

A.32. Alfvénic modes

This corresponds to the first order of perturbations in η . We suppose for Alfvénic waves that $y \ll h$, w and also $d/dx \gg V$. The system governing the Alfvénic waves is

$$\frac{d^2 h_A}{dx^2} + \frac{1}{2} \frac{d\widetilde{w}_A}{dx} = -\frac{c_1 \alpha \sigma^2}{3 \cos^2 \theta} h_A \quad (\text{A.36})$$

$$\frac{d^2 \widetilde{w}_A}{dx^2} - \frac{m^2}{2 \cos^2 \theta} \frac{dh_A}{dx} = -\frac{c_1 \alpha \sigma^2}{3 \cos^2 \theta} \left(\widetilde{w}_A + \frac{m^2 q_A}{c_1 \sigma^2 V} \right) \quad (\text{A.37})$$

$$\frac{dq_A}{dx} = V \left(\frac{\widetilde{w}_A}{\sin^2 \theta} - \frac{c_1 \sigma^2}{2 \cos^2 \theta} h_A \right) \quad (\text{A.38})$$

To solve this system we use a WKBJ approach with the form

$$h_A, \widetilde{w}_A \sim \exp \left\{ i \int^x k dx \right\} \quad (\text{A.39})$$

k obeys the following relation of dispersion

$$(k_A^2 - k^2) \left(k_A^2 - k^2 + \frac{m^2}{4 \cos^2 \theta} \right) = 0 \quad (\text{A.40})$$

with

$$k_A = \sqrt{\frac{c_1 \alpha \sigma^2}{3 \cos^2 \theta}} \gg 1. \quad (\text{A.41})$$

We keep only solutions which propagate inwards. One has, then, two kinds of solutions

– solution with $k = k_A$

$$S_A^1 = \left(0, \frac{iV c_1 \sigma^2}{2k_A \cos^2 \theta}, 1, ik_A, 0, \frac{-m^2}{2 \cos^2 \theta} \right) \quad (\text{A.42})$$

– solution with $k = \sqrt{k_A^2 + m^2/(4 \cos^2 \theta)}$

$$S_A^2 = \left(\frac{iV c_1 \sigma^2}{\Gamma_1 k m^2}, \frac{V c_1 \sigma^2}{m^2}, \frac{-2ik \cos^2 \theta}{m^2}, \frac{2 \cos^2 \theta k_A^2}{m^2}, -1, 0 \right). \quad (\text{A.43})$$

Then, at the base of the magnetic layer $x = x_{\text{fit}}$ the inner boundary condition write as

$$C_p S_p + C_A^1 S_A^1 + C_A^2 S_A^2 = C_1 S_1 + C_2 S_2 + C_3 S_3 \quad (\text{A.44})$$

can be written as the following system of algebraic linear equations

$$\begin{pmatrix} y_1 & y_2 & y_3 & -y_A^1 & -y_A^2 & -y_p \\ q_1 & q_2 & q_3 & -q_A^1 & -q_A^2 & -q_p \\ h_1 & h_2 & h_3 & -h_A^1 & -h_A^2 & -h_p \\ \widetilde{f}_1 & \widetilde{f}_2 & \widetilde{f}_3 & -\widetilde{f}_A^1 & -\widetilde{f}_A^2 & -\widetilde{f}_p \\ \widetilde{w}_1 & \widetilde{w}_2 & \widetilde{w}_3 & -\widetilde{w}_A^1 & -\widetilde{w}_A^2 & -\widetilde{w}_p \\ \widetilde{g}_1 & \widetilde{g}_2 & \widetilde{g}_3 & -\widetilde{g}_A^1 & -\widetilde{g}_A^2 & -\widetilde{g}_p \end{pmatrix} \begin{pmatrix} C_1 \\ C_2 \\ C_3 \\ C_A^1 \\ C_A^2 \\ C_p \end{pmatrix} = 0. \quad (\text{A.45})$$

The solutions with the subscripts 1, 2, 3 are the values at $x = x_{\text{fit}}$ after integration in the boundary layer, and the solutions with the subscript ‘‘A’’ are given by Eq. A.42 and A.43. Requiring that the determinant of the matrix in Eq. A.45 is zero, one obtains the function $\mathcal{F}(\theta, \omega, m)$.

Appendix B:

The results presented in the previous section are not valid at the pole ($\theta = 0$) and the equator ($\theta = \pi/2$) because of the singular behaviour of the equations. For these two points we need to find two systems of equations.

B.1. The pole

At the pole the Lorentz force vanishes. Therefore, the system of equations reduces to the second order Eq. A.30-A.32 (i.e. the system for radial p-modes in the non-magnetic and adiabatic case)

B.2. The equator

At the equator the Lorentz Eq. 6-8 gets a simpler expression

$$L_r = \frac{3VP_0}{4\alpha R} \left(\frac{d^2 y}{dx^2} + im \frac{dw}{dx} \right) \quad (\text{B.1})$$

$$L_\theta = 0 \quad (\text{B.2})$$

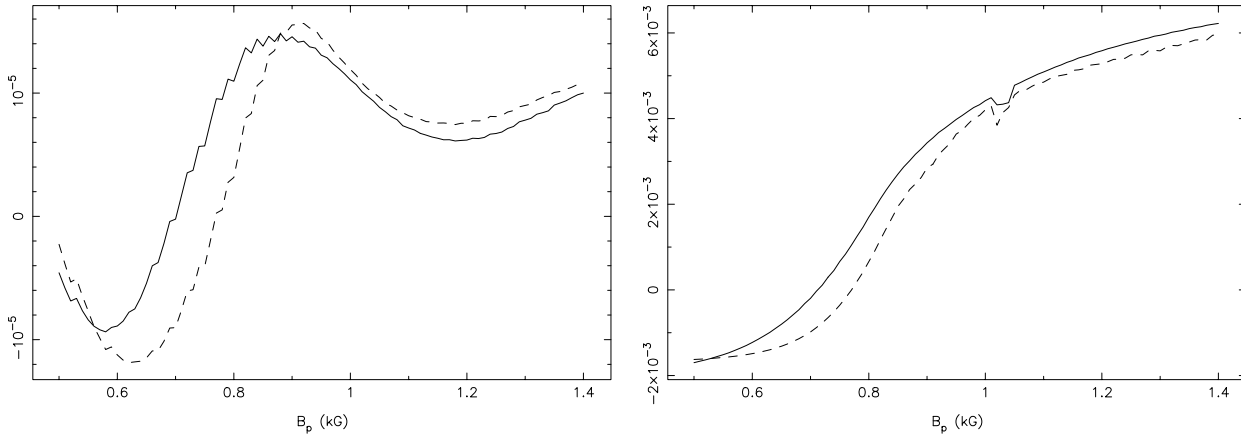


Fig. C.1. Relative differences between the numerical solution for the real frequency (left) and the imaginary frequency (right) with the frequency calculated with Eq. C.1 and Eq. C.2; for the mode $\ell = 1, m = 0$ (full) and $\ell = 1, m = 1$ (dashed) in Fig. 6.

$$L_\phi = \frac{3VP_0}{4\alpha R} \text{Im} \frac{dy}{dx}. \quad (\text{B.3})$$

It can be shown that the system at the equator reduces to the second order

$$\frac{dy}{dx} = \frac{-q}{\Gamma_1} \left(1 - \frac{m^2 \Gamma_1 A}{c_1 \sigma^2 V B} \right) + \frac{m^2 y}{c_1 \sigma^2 B} \quad (\text{B.4})$$

$$\frac{dq}{dx} = \frac{Vq}{A} \left(1 - \frac{m^2 A}{c_1 \sigma^2 V B} \right) + \frac{c_1 \sigma^2 V y}{A} \left(1 - \frac{m^2}{c_1^2 \sigma^4 B} \right) \quad (\text{B.5})$$

with

$$A = 1 + \frac{3V}{4\alpha \Gamma_1} \quad (\text{B.6})$$

$$B = 1 + \frac{3m^2}{4c_1 \sigma^2 \alpha}. \quad (\text{B.7})$$

Appendix C:

The formula Eq. 33 provides a good test for numerical calculations. Once the numerical solution is found the eigen vectors are injected in the following formulas Eq. C.1-C.2 which leads to another evaluation of the frequencies. We neglect the terms corresponding to B since the eigen frequencies corresponds to the oscillations below x_{fit} , i.e. where the dynamical effect of B is negligible compared with the effect of gas pressure.

We give hereafter the formulas for ν_R and ν_I obtained by taking the real and the imaginary part of Eq. 33.

$$\begin{aligned} & 4\pi^2 \nu_R^2 \int_M \left| \vec{\xi} \right|^2 dm = \\ & \text{Re} \left(\oint_S \left(\delta p - \vec{\xi} \cdot \vec{\nabla} p_0 + \rho_0 \Phi_1 \right) \xi_r^* dS \right) \\ & + \text{Re} \left(\int_V \left\{ \frac{|\delta p|^2}{\Gamma_1 p_0} + \vec{\xi} \cdot \vec{\nabla} \ln \rho_0 \vec{\xi}^* \cdot \vec{\nabla} p_0 \right\} dV \right) \\ & + \text{Re} \left(\int_V \left\{ \rho_0 \Phi_1 \left(\frac{\delta p^*}{\Gamma_1 p_0} - \vec{\xi}^* \cdot \vec{\nabla} \ln \rho_0 \right) \right\} dV \right) \\ & - \left(\int_V \left\{ 2 \text{Re} \left(\frac{\delta p^*}{\Gamma_1 p_0} \vec{\xi} \cdot \vec{\nabla} p_0 \right) \right\} dV \right) \end{aligned} \quad (\text{C.1})$$

$$8\pi^2 \nu_R \nu_I \int_M \left| \vec{\xi} \right|^2 dm = W_1 + W_2 + W_3 + W_4 \quad (\text{C.2})$$

with

$$W_1 = \text{Im} \oint_{S_{\text{fit}}} (\delta p) \xi_r^* dS \quad (\text{C.3})$$

$$W_2 = \text{Im} \oint_{S_{\text{fit}}} (\rho_0 \Phi_1) \xi_r^* dS \quad (\text{C.4})$$

$$W_3 = \text{Im} \int_M \Phi_1 \left(\frac{\delta p^*}{\Gamma_1 p_0} \right) dm \quad (\text{C.5})$$

$$W_4 = -\text{Im} \int_M \Phi_1 \left(\xi_r^* \frac{d \ln \rho_0}{dr} \right) dm. \quad (\text{C.6})$$

The relative differences between the numerical solutions of ν_R and ν_I with the frequencies calculated with Eq. C.1 and Eq. C.2 are given in Fig. C.1. We see that the consistency of the calculation are better than 10^{-5} for the real part and better than 0.01 for the imaginary part, for the mode $\ell = 1, m = 0$ and $m = 1$.

References

- Babcock H.W., 1947, ApJ 105, 105
 Borra E.F., Landstreet J.D., Mestel L., 1982, ARA&A 20, 191
 Cunha M., 1998, Contribution of the Astronomical Observatory Skalnaté Pleso Vol. 27, no. 3, p. 272
 Cunha M., Gough D.O., 1998, In: Provost J., Schmitter F.X. (eds.) Sounding Solar and Stellar Interiors- Poster volume, OCA & UNSA, p. 221
 Campbell C.G., Papaloizou J.C.B., 1986, MNRAS 220, 557
 Dolez N., Gough D., Vauclair S., 1988, In: Christensen-Dalsgaard J., Frandsen S. (eds.) Advances in Helio- and Asteroseismology. Reidel, Dordrecht, p. 291
 Dziembowski W.A., Goode P.R., 1985, ApJ 296, L27
 Dziembowski W.A., Goode P.R., 1986, In: Gough D.O. (ed.) Seismology of the Sun and Distant Stars. D. Reidel Publishing Company, Dordrecht, p. 441
 Dziembowski W.A., Goode P.R., 1996, ApJ 458, 338
 Gautschi A., Saio H., Harzenmoser H., 1998, MNRAS 301, 31
 Kurtz D.W., 1982, MNRAS 200, 807
 Kurtz D.W., 1990, ARA&A 28, 607

- Kurtz D.W., 1992, MNRAS 259, 701
Kurtz D.W., Shibahashi H., 1986, MNRAS 223, 557
Martinez P., 1999, IAU Inform. Bull Var. Stars 4348
Martinez P., Ashoka B.N., Kurtz D.W., Gupta S.K., Chaubey U.S.,
1999, IAU Inform. Bull Var. Stars 4677
- Matthews J.M., 1991, PASP 103, 5
Roberts P.H., Soward A.M., 1983, MNRAS 205, 1171
Shibahashi H., Takata M., 1993, PASJ 45, 617
Unno W., Osaki Y., Ando H., Shibahashi H., 1989 Non-radial oscillations of stars. second edition, University of Tokyo Press